

Corrosion of Carbon Steel in a Synthetic Environment and Kerosene on a System with Continuous Flow

L. D. López León^{1,*}, F. J. Olguín Coca¹, A. L. López León², M. Márquez Casasola¹,
M.A. Baltazar Zamora³, G. Santiago Hurtado³, V. Volpi León¹

¹ Universidad Autónoma del Estado de Hidalgo, Carr. Pachuca- Tulancingo Km 4.5, Colonia Carboneras, Mineral de la Reforma, Hidalgo. C.P. 42184, México.

² Universidad Autónoma de Ciudad Juárez, Avenida del Charro 450 Norte, Colonia Partido Romero, Cd. Juárez, Chihuahua. CP 32310, México.

³ Facultad de Ingeniería Civil - Xalapa, Universidad Veracruzana, Circ. G. Aguirre Beltrán S/N, Lomas del Estadio, Xalapa, Veracruz. CP 91000, México.

*E-mail: luis_lopez@uaeh.edu.mx

Received: 11 February 2015 / Accepted: 2 June 2015 / Published: 28 July 2015

This work studies the behavior AISI 1018 carbon steel in a buffered solution of chlorides with and without hydrocarbon in a continuous flow rate system. For techniques was designed a cell setup of a system continuous flow. The electrochemical techniques used polarization curves and electrochemical impedance spectroscopy. The polarization curves obtained indicated that both the anodic part and the cathodic suffer a significant change with the addition of hydrocarbon. The presence of hydrocarbon in the system increases currents in comparison to the system in absence of hydrocarbon. The EIS technique shows steel has a higher activity in the studied solution presented at low frequencies. The adsorption of corrosive agents prevents the formation and growth of a passive layer of corrosion products. The analysis with XPS showed that the presence of hydrocarbon in the system allows the deposition of several Cl⁻ crystals on the metal surface.

Keywords: AISI 1018 carbon steel, Kerosene, polarization curves, electrochemical impedance spectroscopy, X-ray Photoelectron Spectroscopy.

1. INTRODUCTION

Corrosion control is an outstanding element in the preservation of the integrity of industrial systems in the world, it is clear that in the oil industry facilities where there are susceptible equipment to the phenomenon of corrosion, economic losses are very high, as well the decrease in production, strike plant, deployment of personnel for the control of corrosion, etc. Therefore, if the phenomenon is not controlled, it can lead to very significant economic, human and social losses [1]. Therefore, there is

a need to investigate the corrosion resistance of metallic materials found in the oil industry, which, seeks to give longer life of the equipment used and optimize the operation of process plants, on the other hand, due to the large amount of corrosive environments and materials in contact [2], besides the poor knowledge of the mechanisms of corrosion in the oil industry, it is important to do a systematic study to settle mechanistic differences in both the corrosive medium and in the presence of hydrocarbon [3]. On the other hand, the use of corrosive environments for laboratory evaluations of materials used in the oil industry is mainly focused on the proposed in document NACE 1D196 [4], from which, one can establish if a metallic material is or no effective in the industrial environment. Furthermore, the presence of hydrocarbons in industrial environments is also a determining factor as you can modify the corrosion process by corrosive agents causing undesirable results [5]. So, in order to find the effect of immiscible mixtures on the corrosion of the carbon steel, in this work is studied its behavior in a synthetic environment that may determine whether the corrosion mechanism is affected by the presence of hydrocarbon on a system with continuous flow .That is why it is important to evaluate the flow-controlled in the absence and presence of hydrocarbon in order to establish the effect of flow velocity on the corrosion mechanism system of different systems [6]; and thereby establish possible similarities to real systems (oil pipelines) providing knowledge in the research area of corrosion in the oil industry [7].

2. EXPERIMENTAL

2.1. Experimental Setup

For the electrochemical techniques were used an experimental arrangement and a design of a continuous-flow cell (figure 1).

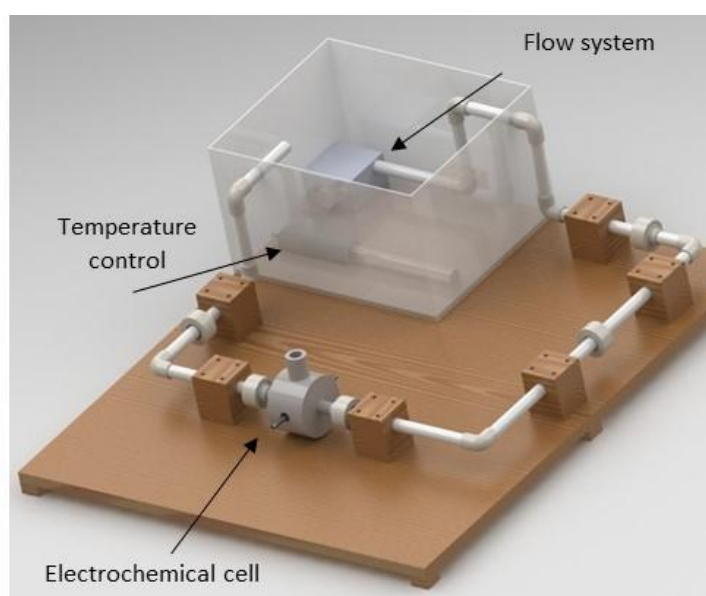


Figure 1. Experimental arrangement.

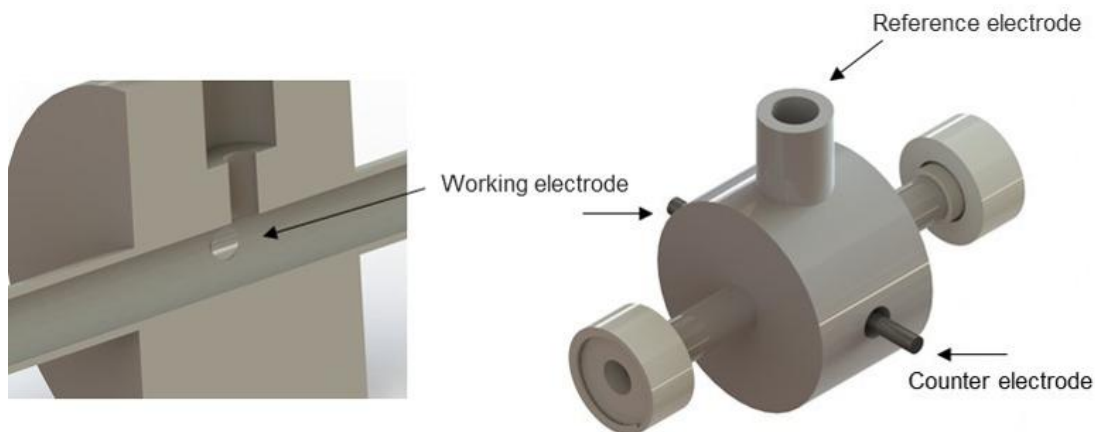


Figure 2. Electrochemical cell.

A three-electrode cell setup was used in electrochemical techniques with a Hg/HgCl(s)/KCl (sat) electrode as reference and a graphite bar as counter electrode. As working electrodes, bars of low AISI 1018 carbon steel (C 0.15/0.20%; Mn 0.60/0.90%; Si 0.15/0.30%; P max. 0.04%; S max. 0.05%) were used and coupled to a Nylamid support (figure 2). Prior to each experiment, the electrode surface was abraded with 280 SiC emery paper. The corrosive environment used was similar as described in the document NACE 1D196 [4,8], with the following composition: 0.03 M Calcium Chloride Dehydrate, 0.01 M Magnesium chloride hexahydrate and 1.82 M Sodium chloride saturated with CO₂ in the absence and presence of hydrocarbon in a ratio 8:2.

The solution was prepared with deionized water, deaerated with high purity nitrogen for 30 min. The following reagents were used (A. R. grade): 99% purity NaCl Baker; 100% purity hexahydrated MgCl₂ Baker, 99% purity dehydrated CaCl₂ Baker and kerosene (hydrocarbon) from Baker. Once the brine is prepared, it is purged with CO₂ (30 minutes per liter of brine) with a controlled pressure of 0.70 Kg/cm² [9].

All experiments were performed at 49 ± 1 °C and after 10 minutes of immersion of the working electrode, allowing the corrosion potential stabilization and with a flow rate 7 liter per minute [10,11]. The potentiodynamic polarization curves were registered at a scan rate of 0.1mV/s in a potential range between ± 300 mV (vs. o.c.p.) and each curve was obtained from a freshly abraded steel surface. The electrochemical impedance spectroscopy (EIS) measurements were carried out with an amplitude of 10 mV (vs. o.c.p.) and in the frequency range of 10 mHz to 10 kHz. A Potentiostat-Galvanostat Autolab Mod PGSTAT30 with Frequency Response Analyzer (FRA) was used and managed through the software of the same company.

Samples were analyzed (XPS) on the Thermo Scientific Escalab 250Xi using XPS, spectroscopic imaging and depth profiling. Samples were mounted on standard or cut-out holders, with conductive tape. The XR6 monochromated X-ray source was used for XPS analyses. This offers a user-selectable spot size from 200-900 μm. Automated in-lens irises may also be used to reduce the analysis area further, offering a range of 300-20 μm. In these analyses, the 900 μm X-ray spot was used for high sensitivity and rapid analysis, and to ensure good coverage in XPS imaging, and the 400

μm spot was used for depth profiling. All data processing (quantification, peak fitting, profile and image generation, PCA, average spectrum generation) was performed within the Advantage data system.

3. RESULTS AND DISCUSSION

3.1 Curves of polarization (without hydrocarbon)

Figure 3 shows potentiodynamic polarization curves of the studying system depending on the immersion time of the electrode and in the absence of hydrocarbon. Shows that both the anodic and cathodic part are modified, showing that higher currents are obtained by increasing the immersion time of the electrode. The corrosion potential that presents in the system is $-700 \pm 40 \text{ mV}$ vs $\text{Hg}/\text{HgCl}(\text{s})/\text{KCl}(\text{sat})$ (SCE), indicating that the initial surface conditions are nearly the same.

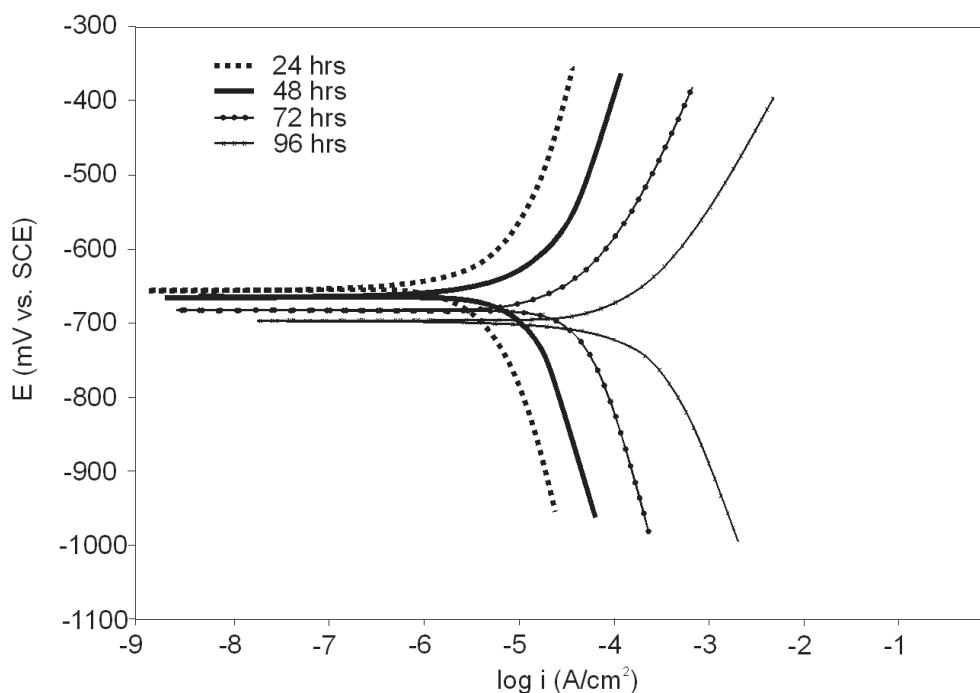


Figure 3. Polarization curves obtained on continued flow system of AISI 1018 carbon steel immersed in a NACE 1D196 solution in the absence of hydrocarbon.

3.2 Curves of polarization (with hydrocarbon)

Figure 4 shows potentiodynamic polarization curves of the studying system in presence of hydrocarbon depending on the immersion time of the electrode. It shows that increasing immersion time, affects both the oxidation and reduction process, showing higher currents by increasing the exposure time of steel. The corrosion potential that presents them in the system is $-700 \pm 40 \text{ mV}$ vs $\text{Hg}/\text{HgCl}(\text{s})/\text{KCl}(\text{sat})$ (SCE), indicating that the initial conditions of the surface are quite similar, even

though the presence of hydrocarbon. On the other hand, presence of hydrocarbon in the system increases the currents in comparison to the system in absence of hydrocarbon.

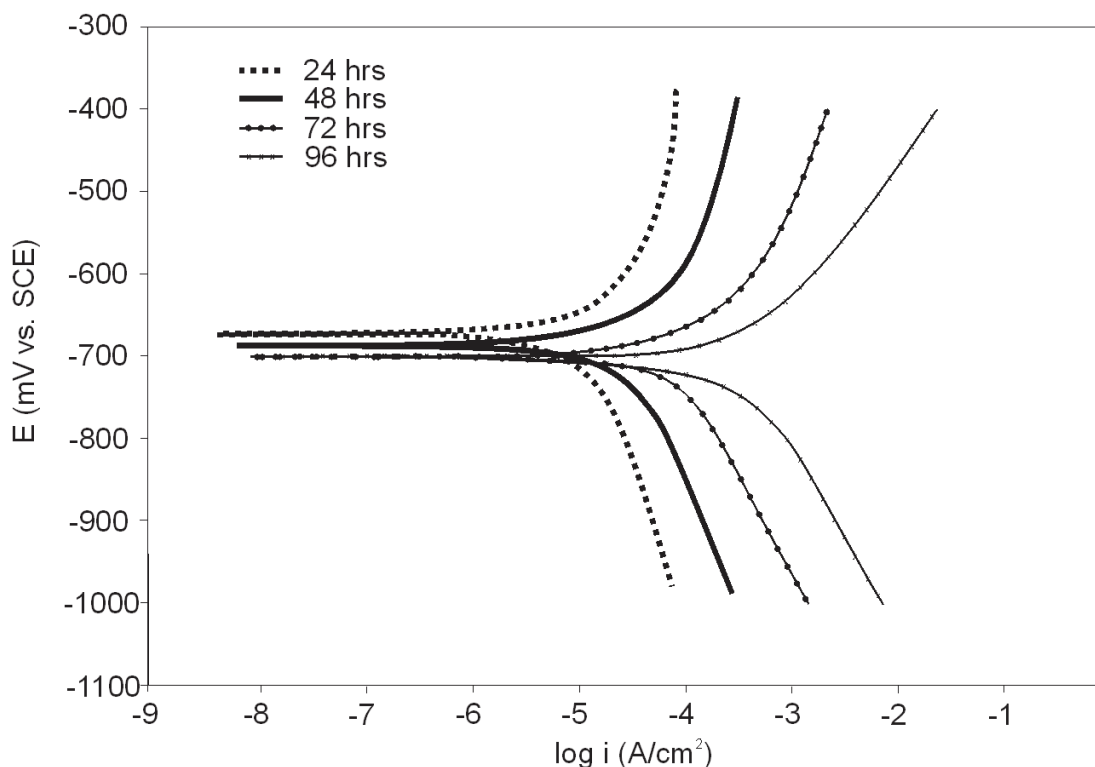


Figure 4. Polarization curves obtained on continued flow system of AISI 1018 carbon steel immersed in a NACE 1D196 solution in presence of hydrocarbon.

It is important to note that the currents shown by the system in the presence of hydrocarbon are higher than that in absence of the latter. Such behavior could be attributed to the presence of a hydrocarbon film in contact with the metal surface, which is constant and that somehow favors the interaction between corrosive species.

3.3 Corrosion parameters obtained from potentiodynamic polarization curves

In Table I, Shows the corrosion parameters obtained for the different systems. Analysis I_{corr} values shows that the presence of hydrocarbon increases the I_{corr} significantly compared to system without hydrocarbon. Furthermore, the values of the anodic slope suggest a higher activity in the surface and a controlled process of charge transfer [12]. In the case of cathodic slope, is important to mention that the values obtained indicate that diffusive processes are still present, favoring the corrosion process in presence of hydrocarbon in the system [13]. The presence of hydrocarbon improve the interaction of the corrosive agents with metal surface [14].

Table I. Corrosion parameters obtained for the different systems.

System		E _{corr} (V)	b _a (V/dec)	b _c (V/dec)	I _{corr} (A/cm ²)
Without hydrocarbon	24 hrs	-0.66	0.0780	-0.290	3.22E-05
	48 hrs	-0.67	0.0872	-0.262	9.73E-04
	72 hrs	-0.69	0.0813	-0.270	1.27E-04
	96 hrs	-0.70	0.0843	-0.262	5.56E-03
With hydrocarbon	24 hrs	-0.67	0.0880	-0.299	8.22E-04
	48 hrs	-0.68	0.0878	-0.272	6.73E-04
	72 hrs	-0.70	0.0891	-0.288	4.67E-03
	96 hrs	-0.70	0.0902	-0.295	1.36E-03

3.4 Electrochemical Impedance behavior of the system without hydrocarbon

Figure 5 shows the Nyquist diagrams of the results of electrochemical impedance spectroscopy (EIS) for the system studied in absence of hydrocarbon and depending on the immersion time of the electrode. The spectra show a similar behavior where the real and imaginary values of impedance increases with increasing time of exposure of carbon steel. In addition, the diffusive processes are very important because they showed semicircles with a linear trend towards lower frequencies [15]. This can be attributed, in first place, by load transfer and subsequently to dissemination of corrosion products into the solution or corrosive species to the surface [16, 17].

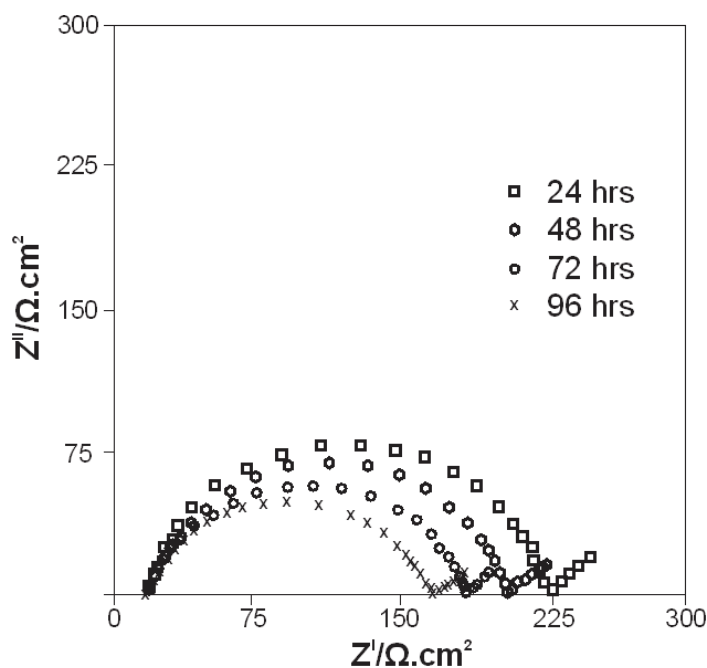


Figure 5. Nyquist diagrams for the system of carbon steel AISI 1018 immersed in a solution NACE 1D196 on a system with continuous flow in absence of hydrocarbon.

3.5 Electrochemical Impedance behavior of the system with hydrocarbon

Figure 6 shows the Nyquist diagrams of the system studied in presence of hydrocarbon and depending on the immersion time of the electrode. It shows that the form of the semicircles changes respect to the system without hydrocarbon, becoming flattened semicircles with an adsorptive tendency, which have been attributed to adsorption or dissolution processes [18]. The impedance values also diminished in comparison with the systems without hydrocarbon indicating higher corrosion rates and favoring the adsorption processes, which is corroborated because the behavior at low frequencies is completely changed respect to the system without hydrocarbon [19, 20, 21]. Thus, it highlights the importance of the study because of the presence of hydrocarbon in a corrosion system can promote the adsorption of corrosive species in a flow continuous system.

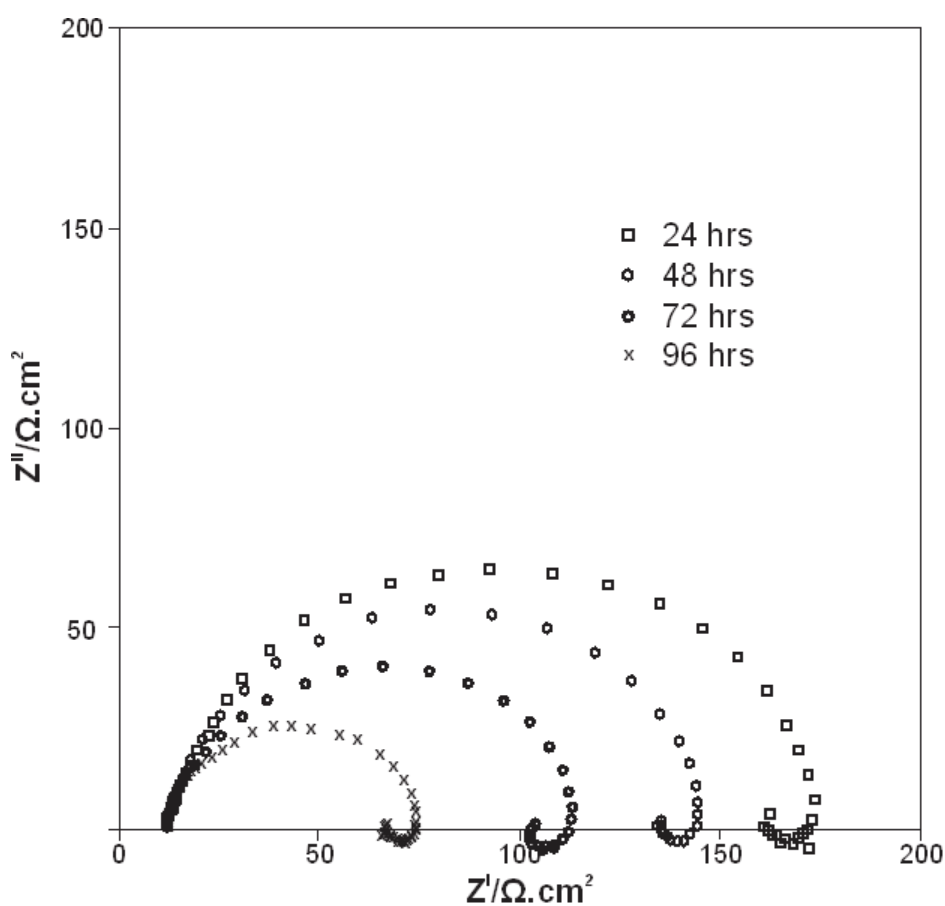


Figure 6. Nyquist diagrams for the system of carbon steel AISI 1018 immersed in a solution NACE 1D196 on a system with continuous flow in presence of hydrocarbon.

Similar to the behavior observed in the Polarization curves, it appears that diffusive processes are very important, showed open semicircles with linear trend toward lower frequencies. This can be attributed primarily to the charge transfer and subsequent to the dissemination of either corrosion products into the solution or corrosive species into the surface.

3.6 Corrosion parameters obtained in the technique of electrochemical impedance spectroscopy

Table II shows corrosion parameters of different systems at different immersion times. The E_{corr} values are very similar this indicate the energy conditions at the start are virtually the same. On the other hand it is observed that the value of resistance to polarization (R_p) decrease as the exposed time of the electrode increase. The polarization resistances for systems in absence of hydrocarbon shows higher values than in the presence of hydrocarbon. This indicate higher corrosion rates in presence of hydrocarbon [22].

Table II. Corrosion parameters obtained in the technique of electrochemical impedance spectroscopy.

System		$E_{\text{corr}} / (\text{V})$	R_s / Ω	R_p / Ω
Without hydrocarbon	24 hrs	-0.65	15.0	152.2
	48 hrs	-0.67	14.7	173.1
	72 hrs	-0.68	15.5	185.6
	96 hrs	-0.71	15.3	209.1
With hydrocarbon	24 hrs	-0.68	12.2	63.8
	48 hrs	-0.69	12.5	103.5
	72 hrs	-0.70	13.2	136.2
	96 hrs	-0.72	13.1	161.7

This behavior suggest the presence of corrosion products in higher level to the system in presence of hydrocarbon, to confirm that, the x-ray Photoelectron Spectroscopy (XPS) analysis were performed, to evaluate the metallic surface after exposed in a corrosive environment.

3.7 X-ray Photoelectron Spectroscopy

For the system without hydrocarbon, the sample was analyzed with the magnetic lens turned off, as the sample was magnetisable. The survey spectrum (Figure 7a) shows C, O, Na, and Fe. Oxygen is removed slowly, and iron increases in intensity. Sodium and manganese are roughly constant in intensity through the profile, while calcium seems to increase slightly [23]. For the system with hydrocarbon (Figure 7b) the sample was analyzed with the magnetic lens turned off, as the sample was magnetisable. The survey spectrum from a lighter area shows C, O, Na, and Fe, along with several other low-concentration elements. Manganese is roughly constant in intensity through the profile, while sodium, calcium and chlorine all increases.

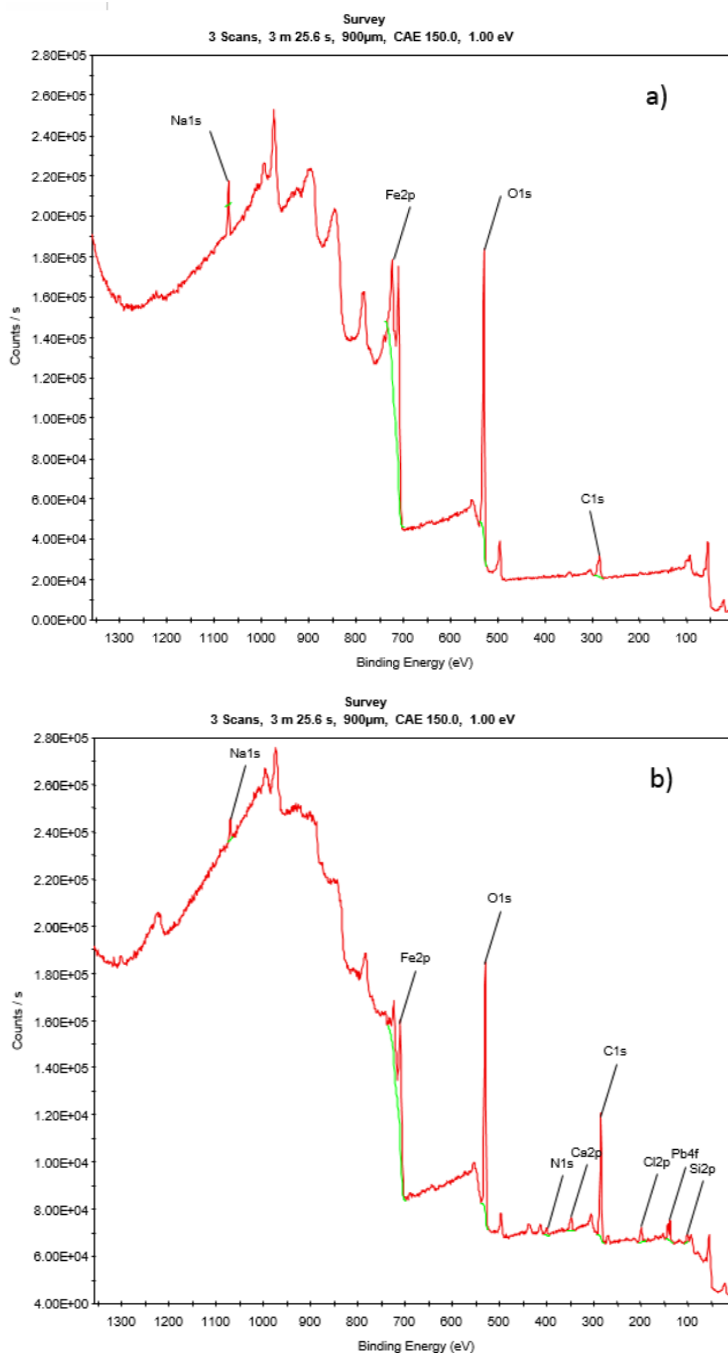


Figure 7. XPS a) Survey Spectrum for the system without hydrocarbon and b) Survey Spectrum for the system with hydrocarbon for the system of carbon steel AISI 1018 immersed in a solution NACE 1D196.

Spectroscopic imaging experiments may be performed to study the structure and chemistry of a sample (figure 8). This entails acquiring sequences of parallel XPS images in small energy steps across an XPS peak region, so that there is spatial information across the whole energy range. This is equivalent to acquiring an image with a spectrum at every pixel. The spectral signal at each pixel is generally quite weak, but by processing part or all of the data set we can get impressive spectroscopic data from the images.

The example shown depicts the F1s spectrum of a microelectronic pad sample (not from this sample set), with five example images from the spectroscopic sequence, which actually included around 40 images. As the energy of acquisition changes, the image structure varies [24]. On the spectral background (first and last images), images show the distribution of that background signal, with the top left pad clearer. On the peak, that pad gains in intensity, and is slightly brighter than the background, which remains at the same level. The spectroscopic image data set is capable of showing the distribution of elemental and chemical states, with high spatial resolution for F1s.

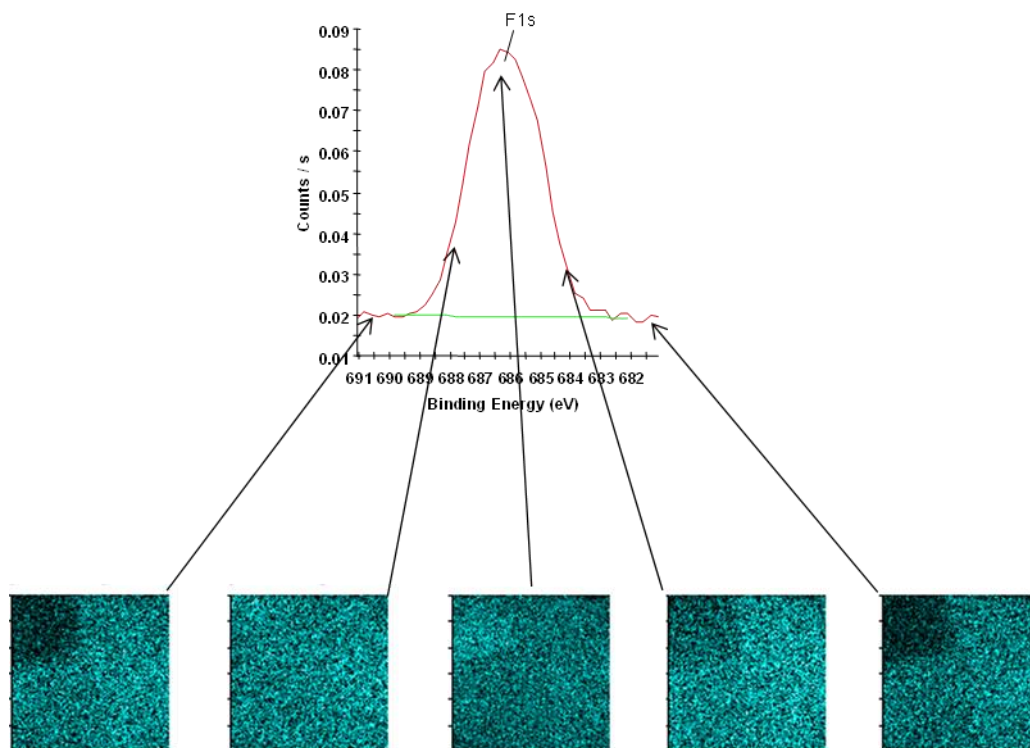


Figure 8. Spectroscopic imaging for the system of carbon steel AISI 1018 immersed in a solution NACE 1D196 with hydrocarbon.

A spectroscopic image analysis of Fe2p was acquired, with a field of view of 1 mm in electrostatic mode (the same as the P-B images) and an analyzer pass energy of 100 eV. The image has a spectrum at each pixel, so a peak was fitted across these spectra to allow peak area measurement. As only one region was measured, a peak area profile image was generated, rather than an atomic % image (figure 9). The area image shows the distribution of intensity of Fe2p across the imaged area. There are a couple of bright spots, ringed in red [25]. These are also ringed on the camera image below. They correlate to a couple of large brown crystals (right) and a cluster of smaller dark crystals (left). The topographical details are also visible, from shadows cast by the crystals, particularly those near the top and center of the image.

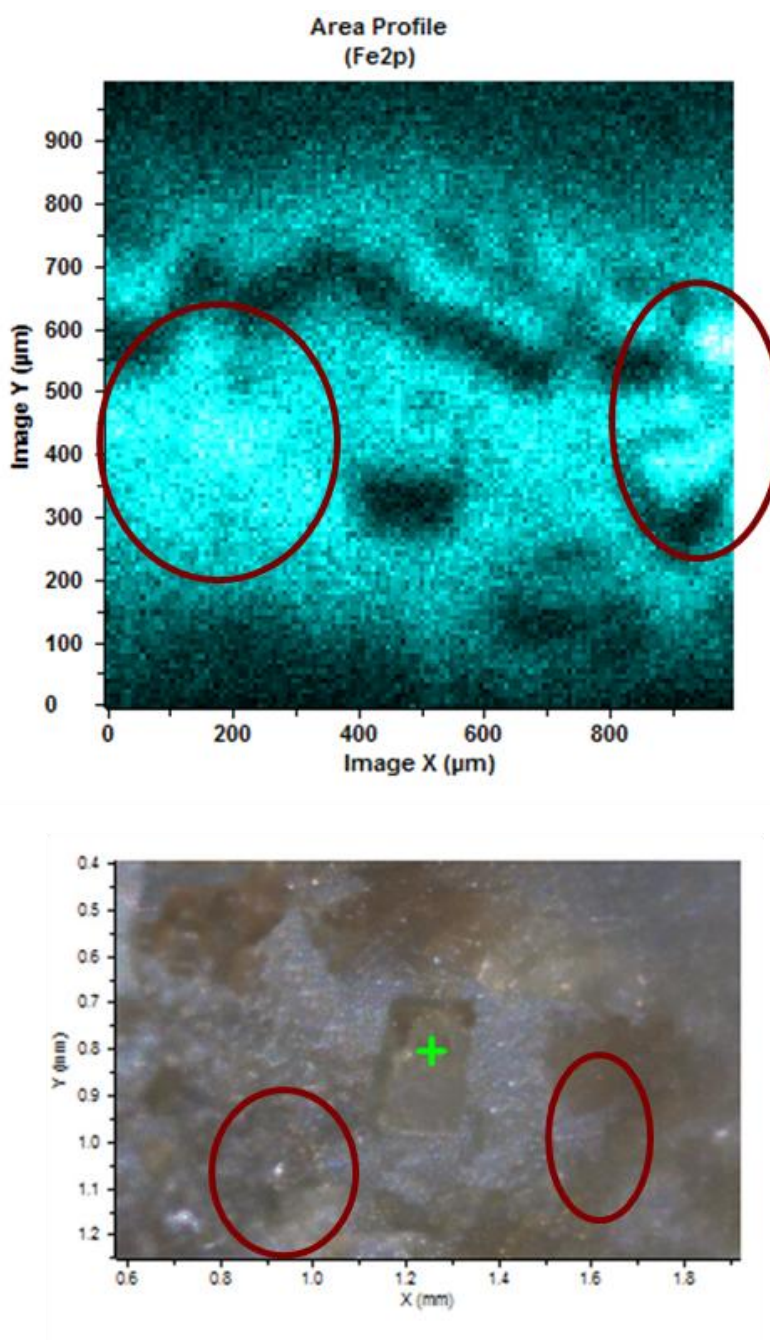


Figure 9. Spectroscopic image analysis of Fe2p for the system of carbon steel AISI 1018.

The presence of a spectrum at each pixel of the image means that there is more information than just the image in the data set (figure 10). Each individual pixel's spectrum is weak, but it is simple to aggregate spectra to give stronger signals [26]. The Advantage data system allows a user to draw rectangular areas on a peak area or at. % image, outlining features of interest. The spectra from all pixels inside these areas are averaged together to yield spectra representative of the selected regions. This has been done for three locations on the sample – the brown crystals (blue box), dark crystal cluster (red box) and central NaCl crystal (orange box). The spectra from the red and blue regions are very similar, indicating that these crystals have similar iron chemistry [27]. The orange box has virtually no iron signal, confirming that the crystal is quite pure NaCl.

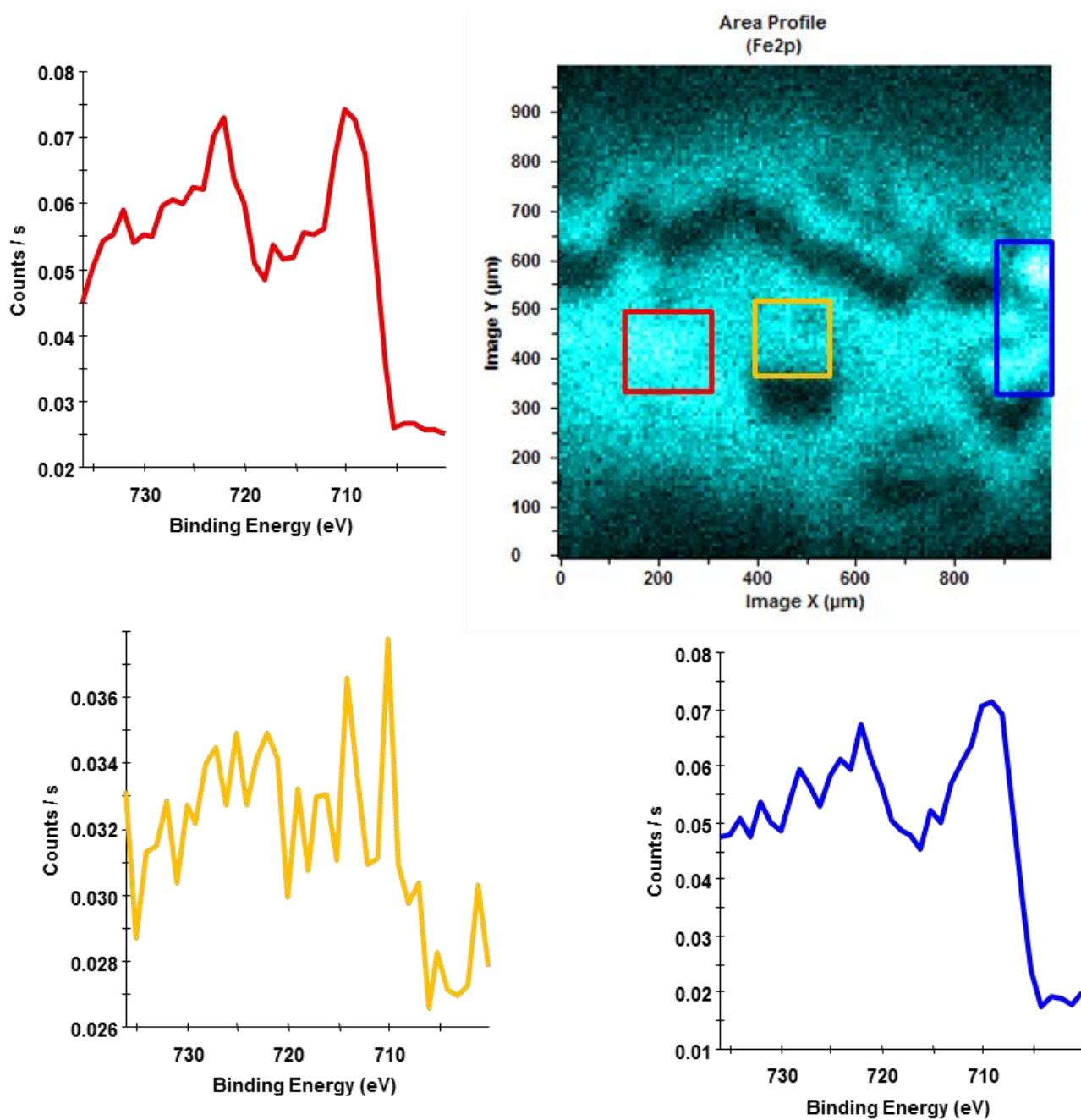


Figure 10. Individual pixel's spectrum for the system of carbon steel AISI 1018 immersed in a solution NACE 1D196 with hydrocarbon immersed in a solution NACE 1D196 with hydrocarbon.

4. CONCLUSIONS

Potentiodynamic polarization curves, showing that the currents obtained are higher for the different systems with the presence of hydrocarbon because affects both the oxidation and reduction process, showing higher currents by increasing the exposure time of steel, however, the diffusive processes are still present in the system.

The use of electrochemical impedance spectroscopy technique shows that the interaction of the hydrocarbon modifies the corrosion process; also, the impedance values also diminished in comparison with the systems without hydrocarbon indicating higher corrosion rates, favoring the adsorption processes it is observed that there are adsorptive processes favoring the arrival of corrosive agents to the metal surface.

Through XPS is observed that interaction of chlorides with metal under different conditions, is increased with the presence of hydrocarbon by considerably modifying the corrosion rate of the system.

ACKNOWLEDGEMENTS

Authors thank to PROMEP by the financial support to the project and to UAEH for the financing resources.

References

1. S. Rossi, F. Deflorian, F. Venturini, *J. Mater. Process. Technol.* 148 (2003), 301-309.
2. E.E. Oguzie, *Corros. Sci.* 49 (2007), 1521- 1539.
3. Kedam M., Mattos O. R., Takenouti H, *J. Electrochem. Soc.* 128 (1981), 257- 266.
4. NACE ID196 "Laboratory Test Methods for Evaluating Oilfield Corrosion Inhibitors", National Association of Corrosion Engineers (1996).
5. K. Magne, *J. Disp. Sci. and Tech.* 27 (2006), 587-597.
6. MA Migahed, IF Nassar, *Electrochim. Acta.* 53 (2008), 2877-2882.
7. MA Migahed, Ahmed A Farag, SM Elsaed, R Kamal, H Abd El-Bary, *Chem. Eng. Commun.* 199, (2012), 1335-1356.
8. MAM Ibrahim, SS Abd El Rehim, MM Hamza, *Mater. Chem. Phys.* 115 (2009), 80-85.
9. Q. B. Zhang, Y. X. Hua, *Electrochim. Acta.* 54 (2009), 1881-1887.
10. Demet Cetin, Mehmet Levent Aksu, *Corros. Sci.* 51 (2009), 1584–1588.
11. F. Beck, U. A. Kruger, *Electrochim. Acta.* 41 (1996), 1083.
12. Congmin Xu, Yaoheng Zhang, Guangxu, *Chinese J. Chem. Eng.* 14 (2006), 829-834.
13. M. M. Singh and A. Gupta, *Corrosion.* 56 (2000), 371-379.
14. Meng Liu, Jianqiu Wang, Wei Ke, En-Hou Han, *J. Mater. Sci. Technol.* 30 (2014), 504-510.
15. C.P Gardiner, R.E Melchers, *Corros. Sci.* 44 (2002), 2665-2673.
16. MA Amin, SS Abd El-Rehim, EEF El-Sherbini, RS Bayoumi, *Electrochim. Acta.* 52 (2007), 3588-3600.
17. AR Sathiya Priya, VS Muralidharan, A Subramania, *Corrosion.* 64 (2008), 541-552.
18. Y. Larabi, M. Harek, M. Traisnel, A. Mansri, *J. Appl. Electrochem.* 34 (2004), 833-839.
19. MM Verdian, K Raeissi, M Salehi, *Corros. Sci.* 52 (2010), 1052-1059.
20. Harvey J. Flitt, D. Paul Schweinsberg, *Corros. Sci.* 47 (2005), 3034-3052.
21. Y. Yan, W. Li, L. Cai and B. Hou, *Electrochim. Acta.* 53 (2008), 5953-5960.
22. M. Mouanga, P. Bercot, J.Y. Rauch, *Corros. Sci.* 52 (2010), 3984-3992.
23. M. El Azhar, M. Traisnel, B. Mernari, L. Gengembre, F. Bentiss, M. Lagrenée, *Surf. Sci.* (2012) 185-197.
24. M. Bobina, A. Kellenberger, J. Millet, C. Muntean, N. Vaszilcsin, *Corros. Sci.* 69 (2013), 389-395.
25. V. Di Castro, S. Ciampi, *Surf. Sci.* 331 (1995), 294-299.
26. Wen-fei LI, Yan-jun ZHOU, Yan XUE. *J. Iron. Steel. Res. Int.* 19 (2012), 59-65.

27. F. Zucchi, G. Trabanelli, G. Brunoro, *Corros. Sci.* 33 (1992), 1135-1146.

© 2015 The Authors. Published by ESG (www.electrochemsci.org). This article is an open access article distributed under the terms and conditions of the Creative Commons Attribution license (<http://creativecommons.org/licenses/by/4.0/>).